Multiphysical Modeling of Calcium Carbonate Transportation in UV Disinfection in Water Treatment

Beibei Z. Sun, and Ernest R. Blatchley*
Civil Engineering, Purdue University
*Corresponding author: 550 Stadium Mall Drive, West Lafayette, IN 47907-2051, blatch@purdue.edu

Abstract: A 2-D multi-physical model was developed to predict fouling problem of calcium carbonate in UV disinfection process using a computational fluid dynamics software called COMSOL. Momentum, heat, and mass transport were linked together to simulation fouling behavior. The simulation result of fouling accumulation was compared with experimental measurements and other simulation results. It showed that COMSOL multi-physical model predicted well in agreement with experimental observations.

Keywords: UV disinfection, fouling, calcium carbonate accumulation, COMSOL, CFD

1. Introduction

Mineral precipitation on to the quartz surface of the lamp jackets in UV disinfection process (fouling) has been recognized as a major problem for UV radiation delivery during disinfection operation. Fouling behavior was observed to be induced thermally and influenced by hydraulic character of the UV disinfection configuration. Fouling process involves momentum, heat, and mass transport within the treated water.

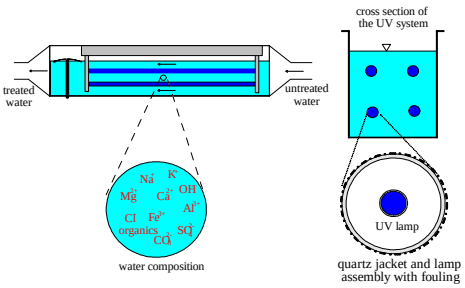

Figure 1. 4-lamp UV disinfection reactor employed in the laboratory experiments (Lin *et al*., 1999a).

A multiphysical modeling software, COMSOL, was used as the tool to simulate this fouling behavior. This model was developed to predict the accumulation of $CaCO_3$ at the quartz water interface. As such, model results could be compared with actual measurements of Ca accumulation at the interface. Figure 1 demonstrates the scheme of the fouling experiment conducted by a previous research group member. The model prediction agrees well with the experimental measurements.

2. Use of COMSOL Multiphysics

In calcium carbonate precipitation, equilibrium between the solid phase and the aqueous (liquid) phase are represented by the solubility product K_{SP} and the dissociation constant of carbonic acid K_{21} which are both functions of temperature.

$$Ca^{2+} + 2HCO_3^- \xleftarrow{K_{SP},K_{21}} CaCO_{3(s)} + H_2CO_3^*$$

Calcium carbonate precipitation is a surface controlled process and removal of calcium from solution was defined by Nancollas and Reddy (1971) and Wiesherst *et al.* (1975) as below:

$$\frac{-d[Ca^{2+}]}{dt} = k_b \times S_a \times \left([Ca^{2+}][CO_3^{2-}] - \frac{K_{SP}(T)}{f^2} \right)$$

The governing equations of momentum transport in the control region at steady state are:

$$\rho\vec{u}\cdot\nabla\vec{u} = \nabla\cdot\left[-P\vec{I} + \eta\left(\nabla\vec{u} + (\nabla\vec{u})^T\right)\right] \quad ,$$

and

$$\nabla\cdot\vec{u} = 0$$

Where, ρ = fluid density,

$\vec{u}$ = velocity,

P = pressure,

η = dynamic viscosity.

The boundary conditions are described as below.

At inlet, $\vec{u} = \vec{u}_0$, which means the velocity at the inlet is the approaching velocity to the reactor.

At all fluid:solid interfaces, a no-slip condition is assumed to apply: $\vec{u} = 0$.

At the outlet, $P_0 = 0$, which implies that no external pressure is applied on the fluid at the outlet.

Where, $\vec{n}$ = normal vector,

P_0 = outlet pressure.

In bulk water, a wall condition applies: $\vec{n} \cdot \vec{u} = 0$, which means no momentum is transported through the wall.

Heat transport in the control region is governed by convection and conduction, where the governing equation at steady state is:

$$\nabla \cdot (-k\nabla T) = Q - \rho C_P \vec{u} \cdot \nabla T$$

Where, T = temperature,

k = thermal conductivity,

C_P = heat capacity,

Q = heat source,

The boundary conditions are described as below.

At inlet: $T = T_0$, which means the temperature of the fluid at inlet equals the initial temperature of the fluid.

On the interface: $-\vec{n} \cdot \vec{q} = q_0$ (heat flux through the quartz sleeves generated from the lamps), and $\vec{q} = -k\nabla T + \rho C_P T \vec{u}$ (heat is then dissipated through the fluid and related to the flow velocity).

At the outlet, convective flux applies: $\vec{n} \cdot \vec{q} = 0$ (no heat flux at the outlet), and $\vec{q} = -k\nabla T$ (heat is dissipated through the fluid).

In bulk water, thermal insulation applies: $\vec{n} \cdot \vec{q} = 0$ (no heat generated), and $\vec{q} = -k\nabla T + \rho C_P T \vec{u}$ (heat is then dissipated through the fluid and related to the flow velocity).

Mass transport in the control region is governed by convection and diffusion. The governing equations at steady state are:

$$\nabla \cdot (-D\nabla C_1) = R - \vec{u} \cdot \nabla C_1 \quad , \quad \text{and}$$

$$C_1(t_0) = C_1$$

Where, D = diffusivity,

C = concentration of the species,

R = reaction rate = $n_l k_b S_a \left(K_{21}(T) \frac{C_1 C_2^{\,2}}{C_3} - \frac{K_{SP}(T)}{f^2} \right)$

Where the indices l = 1, 2, and 3 corresponding to the aqueous phase Ca^{2+}, CO_3^{2-}, and H_2CO_3* respectively;

$K_{2l} = K_2/K_1$;

n_l = stoichiometric coefficients, -1 for Ca^{2+}, -2 for HCO_3^-, and +1 for H_2CO_3* respectively.

The boundary conditions are described as below.

At inlet: $C = C_0$, which means the concentration of the species at inlet equals the initial concentration in the fluid.

On the interface: $-\vec{n} \cdot \vec{N} = 0$ (no mass flux through the interface), $\vec{N} = -D\nabla C + C\vec{u}$ (mass diffuses into the fluid and is influenced by the flow of the fluid), and

$$\vec{N_0} = (-n_l)k_i \left(K_{21}(T) \frac{C_1 C_2^{\,2}}{C_3} - \frac{K_{SP}(T)}{f^2} \right) \quad ,$$

where $\vec{N}$ represents mass flux.

At outlet, convective flux applies: $\vec{n} \cdot \vec{N} = 0$ (no mass flux at outlet).

In bulk water, insulation applies: $\vec{n} \cdot \vec{N} = 0$ (no mass flux through the wall).

A multi-physics model of this behavior has been developed using COMSOL. This model was developed to simulate the accumulation of $CaCO_3$ at the quartz water interface. As such, model results could be compared with actual measurements of Ca accumulation at the interface, as well as the results of numerical simulations presented by Lin *et al.* (1999c). The results of these preliminary simulations are presented below as a series of (velocity, temperature, concentration, saturation index) field simulations for the region of the flowing fluid located immediately adjacent to the quartz:water interface. These results from the simulation were from the 2-D simulation.

3. Results

Figure 2 illustrates the velocity field for the region in the vicinity of the quartz:water interface for conditions corresponding to an

approach velocity of 5 cm/s. These conditions were representative of one of the conditions actually employed in field experiments. The simulation illustrates the development of a momentum boundary layer as fluid moves down the length of the quartz interface. Again, this reactor system was one in which the lamp/jacket assembly was oriented parallel to the direction of flow. This simulation of fluid behavior is consistent with fundamental principles of fluid mechanics. In this simulation, the momentum boundary layer thickness grew to a value of roughly 1.5 cm. The definition of "boundary thickness" here is based on the definition from Bird et al. (1960) as that distance y for which v_x has dropped to a value of $0.99v_0$.

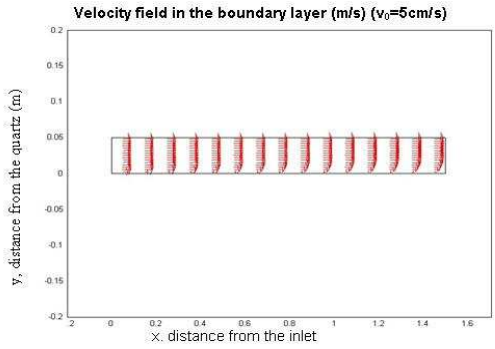

Figure 2. Simulated flow field in the vicinity of a quartz:water interface (y = 0). The flow of water passes from left to right parallel to the orientation of the lamp jacket. The top edge of the computational domain (y = 5 cm) was chosen so as to be inclusive of the mass, heat, and momentum boundary layers.

Figure 3 is a numerical representation of the temperature field for water in the reactor system for a hydraulic loading corresponding to the simulation presented in Figure 2. Inlet water temperature, which was defined as a boundary condition in this simulation, was 12ºC (285 K), corresponding to the conditions of the experiment.

The results of the simulation suggest a maximum increase in water temperature of roughly 4ºC at the quartz:water interface at the downstream end of the reactor system. Also evident is a thermal boundary layer, which grew to a thickness of roughly 1 cm near the downstream end of the system, where the temperature was within 1% of the inlet temperature according to the similar definition described above for the boundary thickness for the momentum transportation.

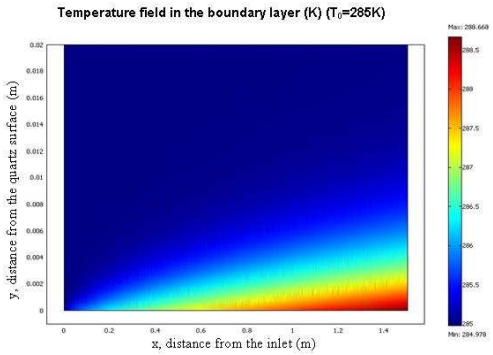

Figure 3. Simulated temperature profile for flow across the boundary layer from the numerical simulation described in Figure 2. The untreated water enters the reactor from left to right with initial temperature of 285 K.

Figure 4 is an illustration of the simulated concentration field for Ca^{2+} in the immediate vicinity of the quartz:water interface. Ca^{2+} concentration is shown to decrease in the direction of flow in the concentration boundary layer, as a result of precipitation reactions that "consume" Ca^{2+} from the liquid phase. The concentration boundary layer grows to a thickness of roughly 5 mm at the downstream end of the system where the concentration of the species approaches 99% of the species initial concentration according to the similar definition of boundary thickness described above for momentum and energy transportation.

A similar analysis was conducted to describe the carbonate (CO_3^{2-}) field (results not shown as the trend is identical to Ca^{2+}). More generally, it is possible to use an analogous approach to simulate the spatial distribution of other ions that are present in solution.

It is important to note that no physical measurements are available to compare with the results of the flow field, temperature field, or concentration field simulations so far because the region of interest is easily interfered with by conventional sampling and analytical instruments. Therefore, it is not possible (at this time) to develop a quantitative assessment of the accuracy of these components of the simulation. However, the boundary layer behavior predictions from these simulations are consistent

with theory, both in terms of the absolute thickness of each layer, and the relative thickness of each layer. As predicted by the model, one would expect the boundary layer thicknesses to follow an order of momentum > heat > concentration based on the relative magnitudes of the fluid viscosity, thermal conductivity, and diffusivity of the aqueous (liquid) medium in which transport is being simulated. This expectation is derived from the theory of momentum, heat, and mass transport where the thicknesses of the three boundary layers related to each other as below.

$$\frac{\delta}{\delta_t} = \mathrm{Pr}^{1/3}, \text{ and } \frac{\delta}{\delta_m} = Sc^{1/3}$$

Where, δ = thickness of the boundary layer in momentum transport,

δ_t = thickness of the boundary layer in heat transport,

δ_m = thickness of the boundary layer in mass transport,

Pr = Prandtl number,

Sc = Schmidt number.

For example, at 20°C, the Prandtl number (Pr) is 6.996, and the Schmidt number (Sc) is 1004 for water. Mathematically, the boundary layer of the momentum transport is the thickest while that of the mass transport is the thinnest.

The results of the ion field simulations for Ca^{2+} and CO_3^{2-} can be combined to develop a saturation index field simulation (see Figure 4). For this presentation, saturation index is defined as the ratio of the ion activity product and the solubility product. Therefore, a saturation index of 1.0 corresponds to a condition of equilibrium between solid-phase $CaCO_3$ and its constituent ions in solution; a saturation index of less than 1.0 represents a condition of subsaturation, while a saturation index greater than 1.0 represents a supersaturated condition. Foulant accumulation would be expected to include $CaCO_3$ in locations corresponding to a saturation index of greater than 1.0; the rate of $CaCO_3$ accumulation would be expected to relate to the extent of supersaturation. For modeling purposes, we assume that the local fouling rate for a given metal:ligand complex is proportional to the local saturation excess, defined as the difference between the ion activity product of the complex and the solubility product.

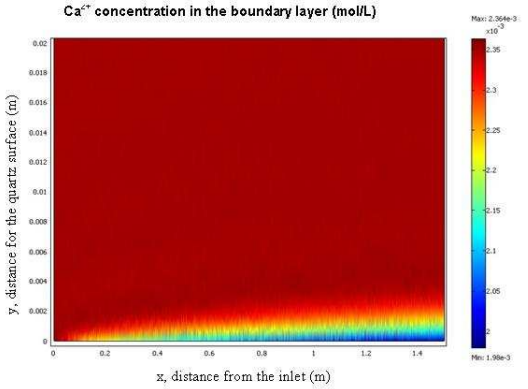

Figure 4. Concentration profile of calcium in the flow across the boundary layer (the same geometry as in figure 2) from the numerical simulation with initial concentration of 2.35 mmol/L in the untreated water entering the reactor.

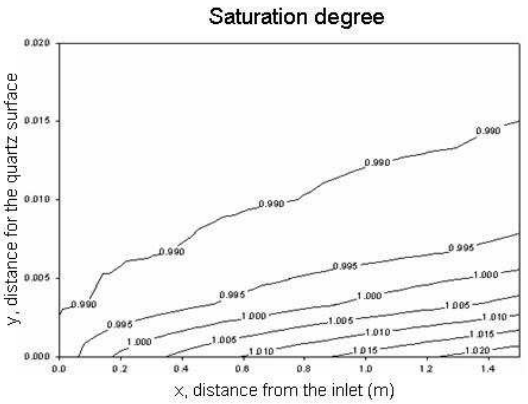

Figure 5. Saturation field index simulation for calcium carbonate across the boundary layer from the numerical simulation. Water enters the system with a saturation index of 0.99. Flow is from left to right.

In the situation illustrated in Figure 5, water enters the system in a condition of slight subsaturation, with respect to $CaCO_3$. As water near the quartz:water interface progresses through the system, it is heated (see Figure 3). As a result, the saturation condition of the water (relative to $CaCO_3$) changes to a condition of slight supersaturation).

The saturation index data are applied to a semi-empirical fouling kinetics sub-model to yield an estimate of the foulant accumulation rate. The accumulation rate for calcium carbonate is expressed by the following equation:

accumulation rate =

$$A_i \times \exp\left(-\frac{E_i}{RT}\right) \times \left(\left[Ca^{2+}\right]\left[CO_3^{2-}\right] - \frac{K_{sp}(T)}{f^2}\right)$$

where,

A_i = pre-exponential constants of reaction rate constants on the quartz:water interface

E_i = activation energy of precipitation (kcal/gmol)

R = gas constant (kcal/[gmol*degree Kelvin])

T = temperature (K)

[ ] = concentration of the ion on the fouling surface (gmol/L)

K_{sp} = solubility product, a dependence on temperature

f = divalent activity coefficient

The linked mass-heat-momentum balance model simulation yields predictions of local foulant ion concentrations, local temperature, and temperature-related solubility product along the quartz:water interface. Based on literature values of A_i and E_i for precipitation of $CaCO_3$, the accumulation rate represented as $CaCO_3$ can be calculated.

The predictions for calcium carbonate accumulation rate are compared with actual field measurements, and a previous simulation conducted by Lin *et al.* (1999c) (see Figure 6). The model described herein yields predictions of foulant accumulation that are in good agreement with experimental measurements, as well as a previous modeling effort. It's shown that COMSOL model prediction yielded a better agreement with the actual measurements.

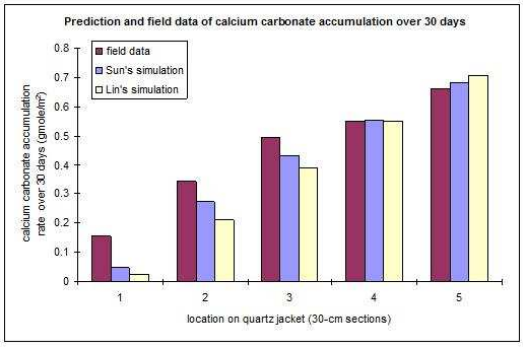

Figure 6. The calculated accumulation for calcium carbonate from the simulation and its comparison with experimental measurement (field data) and previous simulation results (Lin's). Total sum of square error ((measured value – predicted value)^2) is 1.16×10^{-2} in Sun's simulation (proposed model) and 1.84×10^{-2} in Lin's simulation (previous model).

4. Conclusions

COMSOL multiphysics model has demonstrated to be effective for the simulation of thermal-induced calcium carbonate fouling in UV disinfection system. The expansion usage of this numerical simulation tool in the future would allow elaborate examination about how to decrease or eliminate fouling by changing configuration of the operation system, hydraulic parameter, thermal input, and water chemistry.

5. References

Lin, L., Johnston, C.T., and Blatchley III, E.R. "Inorganic Fouling at Quartz:Water Interfaces in Ultraviolet Photoreactors I: Chemical Characterization," *Water Research*, 33:15, 3321-3329 (1999a).

Nancollas, G. H.; Reddy, M. M., "The Crystallization of Calcium Carbonate", *J. Colloid Interface Sci*., vol. 37, no. 4, pp. 824-830, 1971.

Wiecheerst, H. N. S.; Sturrock, P.; Marais, G. V. R., "Calcium Carbonate Crystallization Kinetics", *Water Research*, vol. 9, pp. 835-845, 1975.

Lin, L., Johnston, C.T., and Blatchley III, E.R. "Inorganic Fouling at Quartz:Water Interfaces in Ultraviolet Photoreactors III: Numerical Modelling," *Water Research*, 33: 15, 3339-3347 (1999c).

Bird, B. R., Stewart, W. E., and Lightfoot, E. N. *Transport Phenomena*, John Wiley & sons, New York, (1960).